Wave Structure and Velocity Profiles in Downwards Gas-Liquid Annular Flows

Ivan Zadrazil, Christos N. Markides, Geoffrey F. Hewitt, Omar K. Matar

Department of Chemical Engineering, Imperial College London, SW7 2AZ, UK

Keywords: Two-phase, annular flow, visualisation, Particle Image Velocimetry, Laser Induced Fluorescence

Abstract

The downwards co-current gas-liquid annular flows inside a vertically oriented pipe have been experimentally investigated. The measurements and characterisation were performed using advanced optical non-intrusive laser-based techniques, namely Laser Induced Fluorescence, and Particle Image/Tracking Velocimetry. The investigated conditions were in the range of Re_L = 306 – 1,532 and Re_G = 0 – 84,600. Temporal film thickness time traces were constructed using the Laser Induced Fluorescence images. Based on these, the wave frequency was evaluated using direct wave counting approach and power spectral density analysis. Additionally, qualitative PIV observations revealed the presence of recirculation zones within a wave front of disturbance waves.

Introduction

A number of different flow regimes has been observed for two-phase gas-liquid flows. The type of the flow regime generally depends on the orientation of the pipe as well as on the gas and liquid Reynolds numbers. In the case of vertically oriented pipe, Usui (1989) identified three different flow-regimes: bubbly, slug and annular flow. In this paper we will limit are investigation efforts on downwards annular flow (DAF). This flow can be simply described as a flow of gas in the core of a vertical pipe where the liquid is located in the annulus between the pipe wall and the gas phase. In a special case of DAF, a flow of liquid on the inner surface of the pipe wall can be formed even at zero gas velocity (the so-called 'falling film' case).

The fundamental understanding of the dynamic behaviour of DAFs is not only important from academic but also from the industrial point of view. These flows play a key role in a number of industrial processes, e.g. condensation, distillation or transportation. Better understanding of annular flows can lead to an increase in efficiency as demonstrated by Nakoryakov et al. (1976) who reported that surface instabilities (i.e. waves) can increase a mass-transfer during the absorption of carbon dioxide by water by up to 170%.

DAFs are conventionally described in terms of (i) short lived, small amplitude "ripple" waves, (ii) large amplitude, high speed "disturbance" waves and (iii) a wave-less 'substrate' that is characteristic by its small thickness when compared to the mean film thickness. Disturbance waves are the most complex events that occur in annular flows. They travel at high velocities over slowly moving thin substrate. The liquid in the substrate is then picked-up by the wave, which results in the formation of recirculation zone within the wave front (Mudawar and Houpt, 1993). Due to this feature, disturbance waves are sometimes referred in the literature as to 'rolling' waves. Disturbance waves form ring-like structures that are circumferentially coherent around the pipe, but the thickness of a given wave is not constant around the circumference. Alekseenko et al. (2012) linked the circumferential non-uniformity to the frequency, amplitude and circumferential size of ripples that are formed by the disturbance waves. The presence of disturbance waves is also essential for the liquid entrainment into the gas core (Azzopardi, 1997). The mechanism of the entrainment, as described by Woodmansee and Hanratty (1969), is based on the acceleration of ripples on the crests of disturbance waves.

The structure of annular flows has been usually investigated by using simple photography (Wolf et al., 1996) and conductivity probes (Belt et al., 2010; Zhao et al., 2013). Recently, non-intrusive visualisation techniques, such as Laser Induced Fluorescence (LIF) and Particle Tracking Velocimetry (PIV) have been used to characterise multiphase flows (Liu et al., 2006; Schubring et al., 2010; Morgan et al. 2013). The advantage of these techniques, when compared to the previously used, is that they allow simultaneous qualitative (i.e. imaging) and quantitative characterisation of the multiphase flows. The quantitative analysis can provide information on film thickness, bubble size, wave frequency or velocity distribution within the liquid film.

In this paper we use a combination of non-intrusive, spatiotemporally resolved optical techniques, namely Plannar LIF (PLIF), and Particle Image and Tracking Velocimetry (PIV, PTV) in order characterise downwards co-current gas-liquid annular flows. We will demonstrate that these techniques can be successfully used to obtain both qualitative and quantitative results that can help to understand the phenomena appearing in annular flows.

Nomenclature

d	Pipe diameter (m)
l	Length of the test section (m)

f	Wave frequency (Hz)
u	Speed (m.s^{-1})
Re	Reynolds number (–)
R	Pipe radius (m)
n	Refractive index (–)

Greek letters

δ	Film thickness (m)
μ	Kinematic viscosity (m^2.s^{-1})

Miscellaneous

$\langle X \rangle$	Time-averaged or mean variable
X_S	Superficial variable
X_G	Gas related variable
X_L	Liquid related variable

Experimental Facility

Downwards Annular Flow Laser Observation Facility (DAFLOF) has been used for the presented study. This facility was constructed in order to allow detailed laser visualisation of the gas-liquid multiphase flows – namely downwards annular flow. Figure 1 shows the schematic illustration of the flow facility. DAFLOF consists of l = 3 m long and d = 32 mm fluorinated ethylene propylene (FEP) pipe.

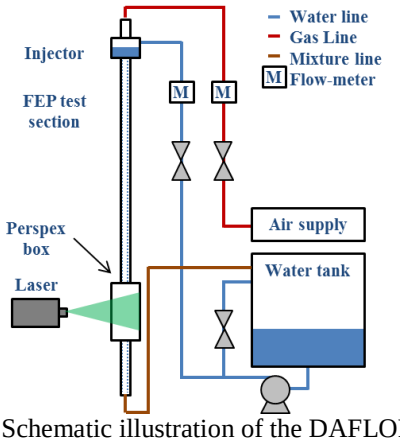

Figure 1: Schematic illustration of the DAFLOF facility.

Air and water were used as the gas and liquid, respectively. A filtered laboratory air supply at 7 bar was used as the source of the gas. Two centrifugal pumps, connected either in series or parallel, were used to circulate the water through a closed loop. An annular liquid film was injected onto the FEP pipe wall using an injector that consists of interconnected bevels. Such an injector provides azimuthally uniform liquid film around the pipe periphery. Additional details of the injector can be found in Zhao et al. (2013). The investigated Reynolds numbers were selected to be in the ranges Re_G = 0 – 84,600 and Re_L = 306 – 1,532. Here the liquid Reynolds number was defined based on the mean film thickness $Re_L = \langle u_L \rangle \langle \delta \rangle / \mu_L$, where $\langle u_L \rangle$ is the mean film velocity, $\langle \delta \rangle$ the mean film thickness and μ_L the kinematic viscosity of water. The gas superficial velocity u_{GS} and the pipe diameter d were used for the calculation of gas Reynolds number $Re_G = u_{GS} d / \mu_G$. The kinematic viscosities of air and water used here were 1.57 10^{-5} and 9.02 10^{-7} m^{2}s^{-1}, respectively.

A special visualisation cell was manufactured, employing a refractive index matching technique, in order to minimise any optical distortions. At the point where the laser visualisation was performed, the FEP tubing was enclosed in a Perspex box with square sides. The inside of the box (i.e. the volume between the FEP tubing and the internal walls of the Perspex box) was filled with de-ionized water. The refractive indices of water and FEP are 1.33 and 1.34, respectively. The visualisation cell was located 2.35 m upstream from the liquid injector.

A PIV system (LaVision GmbH) was used for the visualisation and consecutive analysis of the annular flow. The system comprises a double-pulsed frequency-doubled Nd:YAG laser, having an emission wavelength of 532 nm and frequency 100 Hz. Sheet optics with a divergence of 20º was used to illuminate the annular flow in a 2-D plane. The thickness of the laser sheet at the point of the measurement was approximately 0.1 mm. Two different techniques were employed for the flow visualisation, namely Planar Laser Induced Fluorescence (PLIF) and Particle Image Velocimetry (PIV). Rhodamine-B dye and Rhodamine-B particles (10 µm in diameter) were used for the PLIF and PIV measurements, respectively. The scattered fluorescent light was captured by a mid-speed monochromatic CMOS camera, positioned at 90º to the laser light sheet. A set of 500 images was recorded during each measurement. The resolution and the viewing window of the camera were 1,280 × 1,024 pixels and 29 × 33 mm, respectively. This corresponds to a pixel spatial resolution of 22 µm.

The analysis of the raw PLIF images consisted of the following steps:

1. Binarisation – conversion into black and white equivalents using a threshold approach.
2. Direct measurement of the instantaneous film thickness and evaluation of the mean and Probability Density Function (PDF).
3. Application of a two-pass cross-correlation algorithm to the binarised images. The information of the displacement between consecutive images was then used for the construction of *the temporal film thickness time traces*.
4. Statistical analysis of the temporal film thickness traces – interfacial wave frequency.

Two different methods have been employed to evaluate the interfacial wave frequency f: (i) direct counting of waves larger than 2 and 4×$\langle \delta \rangle$, and (ii) Power Spectral Density (PSD) analysis of the temporal film thickness time traces.

Results and Discussion

The temporal film thickness time traces for the falling films (i.e. Re_G = 0) are shown in Figure 2. The instantaneous PLIF images of the wave fronts (x_1) and the substrate (x_2) for a given condition are also shown in Figure 2. This figure shows that the liquid film undergoes two successive flow regime transitions. For low Re_L (Figure 2(a)) large waves are the dominant features. With increasing Re_L (Figure 2(b)) large waves tend to disappear, however, sinusoidal

frequency ripples occupy the substrate. At the highest investigated Re_L (Figure 2(c))) large waves as well as high frequency ripples cover the substrate. The transition between (a) and (b) occurs at approximately Re_L = 600. The reason for the change in the trends of the temporal film thickness time traces can be the change from laminar to turbulent nature of the falling films. Karapantsios et al. (1989) indeed observed a deviation of the mean film thickness $\langle\delta\rangle$ from the Nusselt relation at Re_L = 500.

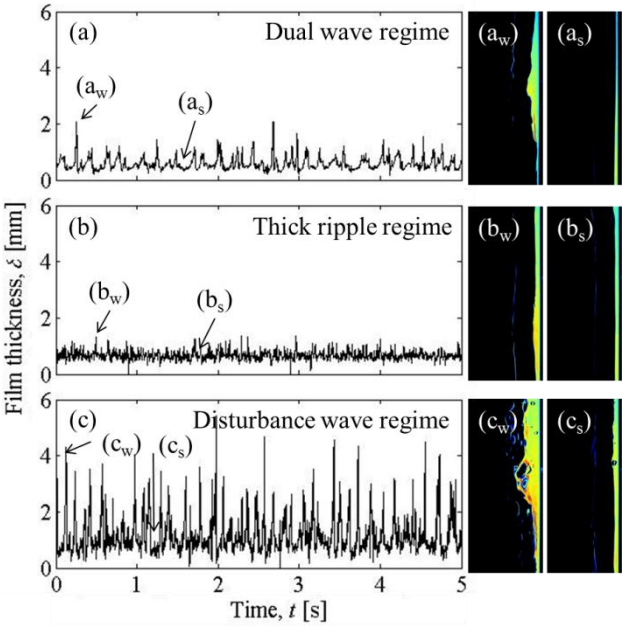

Figure 2: Temporal film thickness time traces and instantaneous raw PLIF images of wave fronts (x_w) and substrates (x_s) for falling films (i.e. Re_G = 0) and Re_L of (a) 306, (b) 613 and (c) 1,532.

In Figure 3, we show the temporal film thickness time traces and the instantaneous PLIF images of downwards annular flows with constant liquid Reynolds number Re_L = 306 and varying gas Reynolds number Re_G = 21,100 – 84,600. Several qualitative observations can be made: (i) increasing Re_G results in increased occurrence of random small amplitude wave structures. Additionally, the frequency of these structures appears to increase with Re_G. (ii) The amplitude and the occurrence of the large waves initially increases with increasing Re_G. However, no large waves can be observed if the Re_G passes a certain threshold. (iii) The thickness of the liquid film decreases with increasing Re_G. This indicates that the liquid film is accelerated by the gas shearing forces and also that liquid entrainment into the gas core does occur. Furthermore, the following observations can be made:

- The amplitude of the large as well as the small waves is not constant over time.
- Large waves do not travel over the liquid film individually, but they consist of a number of smaller waves (i.e. ripples).
- At low Re_L and zero Re_G, the substrate can be described as flat. At high Re_L and non-zero Re_G, the substrate is fully covered by small-amplitude waves.
- Increasing Re_L or Re_G leads to an increase in the complexity of observed waves (i.e. they cannot be described as individual waves).

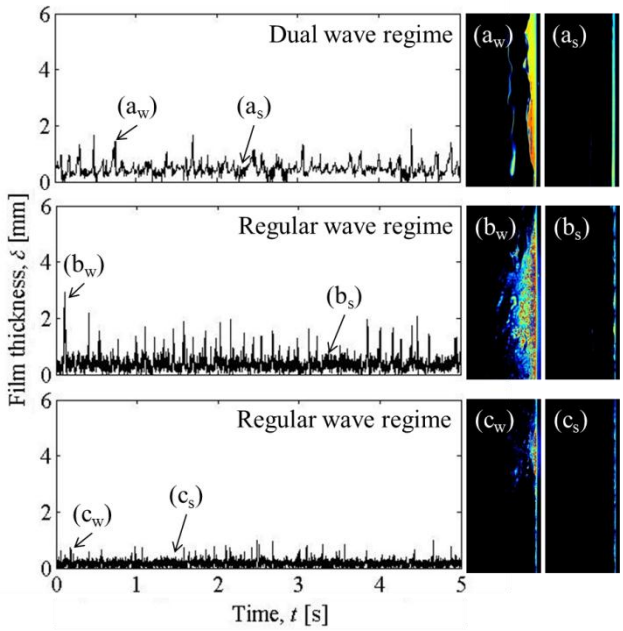

Figure 3: Temporal film thickness time traces and instantaneous raw PLIF images of wave fronts (x_w) and substrates (x_s) for Re_L = 306 and Re_G of (a) 21,100, (b) 42,300 and (c) 84,600.

Four distinctive flow regimes of downwards annular flow were identified during earlier analysis of the presented experimental campaign (Zadrazil et al. 2012). They were identified based on simple qualitative evaluation of the raw instantaneous PLIF images. It can be clearly seen from Figures 2 and 3 that each regime is also specific by a unique topology of the liquid interface (i.e. temporal film thickness time trace).

The interfacial wave frequency was evaluated by a direct counting of waves having an amplitude larger than $2\times\langle\delta\rangle$ (i.e. large ripples) and $4\times\langle\delta\rangle$ (i.e. disturbance waves). These results are presented in Figure 4(a) and (b). It can be seen that the frequency of the waves is strongly dependent on their amplitudes, such as that the frequency decreases with increasing amplitude. In the case of large ripples (Figure 4(a)) the frequency increases with increasing Re_G. The dependency of the frequency of large ripples on Re_L is more complex. In the case of falling films (i.e. Re_G = 0) the wave frequency decreases, reaches a minimum and then increases. This trend follows the change in the flow-regimes, with increasing Re_L the flow regimes change as follows: dual wave -> thick ripple -> disturbance wave regime. Increasing Re_G leads to a sudden change of flow regimes. For the ripple wave regime, the frequency of the large ripples is higher (by a factor of two) when compared to the other observed flow regimes.

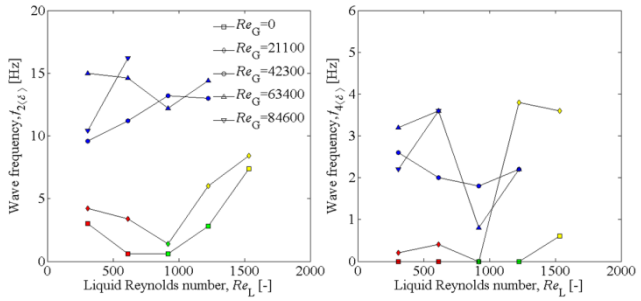

Figure 4: Frequency of (a) large ripples (wave amplitude larger than $2\times\langle\delta\rangle$) and (b) disturbance waves (wave amplitude larger than $4\times\langle\delta\rangle$) as a function of Re_L. The colours indicate different flow regimes: red – dual wave regime, green – thick ripple regime, yellow – disturbance wave regime and blue – regular wave regime.

If we consider the frequency of larger amplitude waves, Figure 4(b), then the trends can also be divided into groups that can be linked to a specific flow regime. In the case of dual wave regime the occurrence of disturbance waves is very rare. These large amplitude waves (i.e. disturbance waves) are completely absent in the thick ripple regime. As the flow regime name suggests, the gas-liquid interphase is occupied by sinusoidal low amplitude waves. Increase in a liquid flow rate (i.e. Re_L) results in a sudden increase in the frequency of disturbance waves – disturbance wave regime. It should be noted that according to Azzopardi (1983) the presence of large waves (i.e. disturbance waves) is essential to the liquid entrainment into the gas phase. Finally, the regular wave regime is characteristic of a frequent occurrence of disturbance waves. These relatively large amplitude waves are thinner than the disturbance waves at lower Re_G. This is caused by a relatively thin nature of these liquid films, $\langle\delta\rangle$ = 0.662 mm for Re_L = 613 (falling film) and $\langle\delta\rangle$ = 0.166 mm for Re_L = 613 and Re_G = 84,600.

Another common way of obtaining the wave frequency is to calculate the power spectra density (PSD). Figure 5(a) and (b) show the PSDs for falling films (Re_G = 0) and constant liquid Reynolds number Re_L = 306, respectively. It is well known that a slope of PSD for a turbulent signal is equal to -5/3. The slope of the investigated DAF film thickness signals is found to be steeper than that of the typical turbulent signal. Nevertheless, this discrepancy is diminishing with increasing both Re_G and Re_L. Modal frequency (i.e. frequency at the maximum power) is sometimes linked to the frequency of disturbance waves. In the case of falling films, the modal frequency can be found in the range of 4 – 9 Hz. It seems that the modal frequency is independent of Re_L but dependent on Re_G. Figure 5(b) shows that, if the gas Reynolds number is increased from 0 to 84,600, the modal frequency also increases from 8 to 25 Hz. Additionally, the power at the modal frequency decreases with increasing Re_G. Opposite trend can be found when Re_L is considered as a variable.

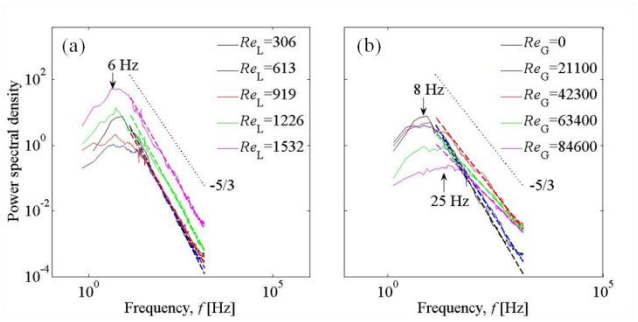

Figure 5: Power spectra density for (a) constant gas Reynolds number Re_G = 0 and (b) constant liquid Reynolds number Re_L = 306.

The modal frequency, extracted from the PSDs, such as those in Figure 5, as a function of Re_G is shown in Figure 6. The trends collapse on a single trend curve, signifying that Re_G is the scaling factor for the modal frequency. Azzopardi (1997) attributed the modal frequency of PSD to the frequency of disturbance waves. Brief comparison of Figures 4 and 6 indicates that the modal frequency (i.e. the frequency of the waves carrying the highest portion of energy) can rather be attributed to small amplitude waves, instead of large amplitude disturbance waves. This means that these small amplitude waves (i.e. ripples) carry the highest amount of energy which contrasts with what was previously assumed (i.e. the energy is mainly transferred by disturbance waves).

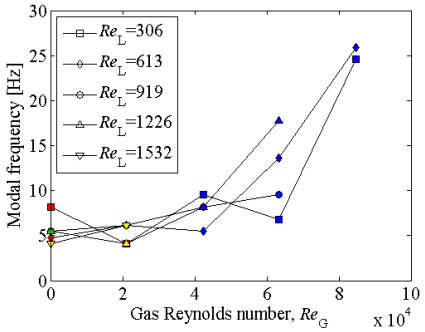

Figure 6: Modal frequency as a function of Re_G. The colours indicate different flow regimes: red – dual wave regime, green – thick ripple regime, yellow – disturbance wave regime and blue – regular wave regime.

Downwards annular flows are highly complex in their structure. Brauner et al. 1987 discussed the existence of interfacial stagnation points that are accompanied by a circulating eddy within the wave (recirculation zone). This occurs when the wave velocity is exceeded by the interfacial velocity. Figure 7 shows instantaneous velocity fluctuations vector maps with superimposed streamlines. The recirculation zones within the disturbance wave fronts are clearly visible and they depict the complex nature of the annular flows.

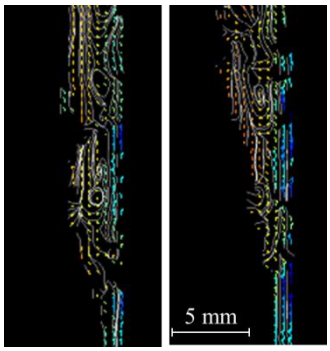

Figure 7: Instantaneous PIV images of wave fronts. Streamlines show the recirculation zones within the waves. The length and colour of the vectors correspond to the magnitude of the velocity fluctuations. The flow conditions for both images are: $Re_G = 0$ and $Re_L = 1532$.

Figure 8(a) and (b) present typical results of the velocity and r.m.s. profiles for Re_G = 0 and 42,300, respectively. The velocity profiles are continuous (i.e. no abrupt change in speed can be observed). Due to the liquid viscous friction, the speed at the vicinity of the wall approaches zero values and gradually increases with distance from the wall. The film velocity increases with increasing both Re_L and Re_G. The velocity profiles at relatively low Re_L and zero Re_G follow theoretical Nusselt velocity profiles and can therefore be described as laminar. However, with increasing Re_L and Re_G, the velocity profiles deviate from the Nusselt predictions and they assume a more turbulent character (i.e. logarithmic profile). The r.m.s. profiles steeply increase in the vicinity of the wall and then reach a plateau.

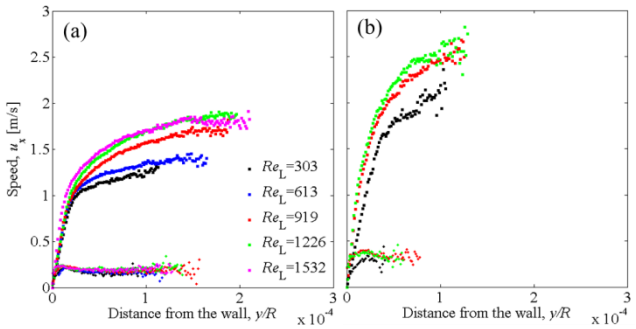

Figure 8: Mean streamwise speed u_x and the r.m.s. as a function of the distance from the wall y/R for (a) $Re_G = 0$ and (b) Re_G = 42,300.

Typically only time-averaged velocity information (i.e. velocity profiles) can be found in the literature. However, temporal information on the liquid films is essential for successful modelling and predictions. Figure 9(a) and (b) show a PTV velocity vector map and instantaneous velocity profiles within a disturbance wave, respectively. It can be seen that both laminar and turbulent features (e.g. parabolic and logarithmic shape of the velocity profiles) can be identified within a single disturbance wave.

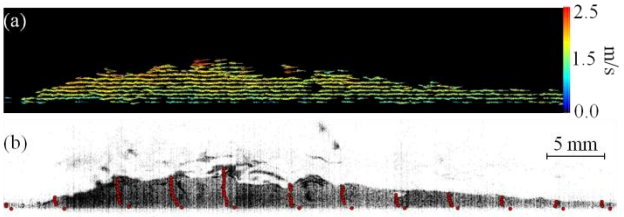

Figure 9: (a) a PTV velocity vector map and (b) instantaneous velocity profiles within a disturbance wave. The flow conditions are: $Re_G = 0$ and $Re_L = 1532$.

Conclusions

Non-intrusive optical techniques, namely PLIF and PIV/PTV, have been used for both qualitative and quantitative characterisation of waves in downwards co-current annular flows. A two pass cross-correlation has been applied on the PLIF images and the temporal film thickness time traces have been constructed. These were used for the evaluation of the wave frequency using (i) direct wave counting and (ii) power spectral density analysis. It was found that ripples (i.e. small amplitude waves) carry the majority of energy, rather than large amplitude disturbance waves. PIV/PTV measurements revealed the presence of recirculation zones within a wave front of a disturbance wave. To the best of our knowledge, this is the first study capturing the recirculation zones in annular flows to such a detail.

References

Alekseenko, S., Cherdantsev, A., Cherdantsev, M., Isaenkov, M. Kharlamov, S. and Markovich, D. Application of a high-speed laser-induced fluorescence technique for studying the three-dimensional structure of annular gas-liquid flow, Exp. Fluids 53, 77–89 (2012).

Azzopardi, B.J. Mechanisms of entrainment in annular two-phase flow, UKAEA Report AERE-R 11068 (1983).

Azzopardi, B.J. Drops in annular two-phase flow, Int. J. Multiphase Flow 23, 1–53 (1997).

Belt, R.J., Van't Westende, J.M.C., Prasser, H.M. and Portela, L.M. Time and spatially resolved measurements of interfacial waves in vertical annular flow, Int. J. Multiph. Flow 36, 570–587 (2010).

Brauner, N., Maron, D.M., and Toovey, I. Characterization of the interfacial velocity wavy thin film flow, Int. Comm. Heat Mass Transfer 14, 293–302 (1987).

Karapantsios, T.D., Paras, S.V. and Karabelas, A.J. Statistical characteristics of free falling films at high Reynolds numbers, Int. J. Multiph. Flow 15, 1–21 (1989).

Liu, L., Matar, O.K. and Hewitt, G.F. Laser-Induced Fluorescence (LIF) studies of liquid-liquid flows. Part II: Flow pattern transitions at low liquid velocities in downwards flow, Chem. Eng. Sci. 61, 4022–4026 (2006).

Morgan, R.G., Markides, C.N., Zadrazil, I. and Hewitt, G.F.

Characteristics of horizontal liquid – liquid flows in a circular pipe using simultaneous high-speed laser-induced fluorescence and particle velocimetry, Int. J. Multiph. Flow, accepted.

Mudawar, I. and Houpt, R.A. Measurement of mass and momentum transport in wavy laminar falling liquid films, Int. J. Heat Mass Transfer 36, 4151–4162 (1993).

Nakoryakov, V.E., Pokusaev, B.G. and Alekseenko, S.V. Stationary two-dimensional rolling waves on a vertical film of liquid, J. Eng. Phys. 30, 517 (1976).

Schubring, D., Ashwood, A.C., Shedd, T.A. and Hurlburt, E.T. Plannar Laser-Induced Fluorescence (PLIF) measurements of liquid film thickness in annular flow. Part I: Methods and data, Int. J. Multiph. Flow 36, 815–824 (2010).

Usui, K. Vertically downward two-phase flow, (II) flow regime transition criteria, J. Nuclear Sci. Tech. 26, 1013–1022 (1989).

Wolf, A., Jayanti, S. and Hewitt, G.F. On the nature of ephemeral waves in vertical annular flow, Int. J. Multiph. Flow 22, 325–333 (1996).

Woodmansee, D.E. and Hanratty, T.J. Mechanism for the removal of droplets from liquid surface by a parallel air flow, Chem. Eng. Sci. 24, 299 (1969).

Zadrazil, I. Markides, C.N., Matar, O.K., Ó Náraigh, L. and Hewitt, G.F.. Characterisation of downwards co-current gas-liquid annular flows. Proc. 7th Int. Symp. Turb. Heat Mass Transf. (THMT'12), Palermo, Italy (2012).

Zhao, Y., Markides, C.N., Matar, O.K. and Hewitt, G.F. Disturbance wave development in two-phase gas-liquid upwards vertical annular flow. Int. J. Multiph. Flow, accepted.